Cancer Nanotechnology

RESEARCH Open Access

Inhibition of PD-L1 and tumor growth in triple-negative breast cancer using a magnetic nanovector with microRNA34a

Seung-Hyun Yang[1,2], Hye Young Son[1,2], Mirae Park[1], Hyun Wook Rho[1], Hwunjae Lee[1,2,4*†] and Yong-Min Huh[1,2,3,5*†]

†Hwunjae Lee and Yong-Min Huh contributed equally to this work.

*Correspondence: hjlee7@yuhs.ac; ymhuh@yuhs.ac

[1] Department of Radiology, College of Medicine, Yonsei University, 50-1 Yonsei-Ro Seodaemun-Gu, Seoul 03722, Republic of Korea
[2] College of Medicine, YUHS-KRIBB Medical Convergence Research Institute, Yonsei University, 50-1 Yonsei-Ro Seodaemun-Gu, Seoul 03722, Republic of Korea
[3] Department of Biochemistry & Molecular Biology, College of Medicine, Yonsei University, Seoul 03722, Republic of Korea
[4] Graduate Program of Biomedical Engineering, College of Medicine, Yonsei University, Seoul 03722, Republic of Korea
[5] Severance Biomedical Science Institute, College of Medicine, Yonsei University, Seoul 03722, Republic of Korea

Abstract

Background: Clinical applications of RNA interference for cancer treatment and immune therapy require the development of simultaneous therapy and imaging systems for microRNA. This research was performed to fabricate the miRNA34a-loaded magnetic nanoparticles and investigate its anticancer effects against triple-negative breast cancer (TNBC) in mice model.

Results: Using two types of polymers to improve their water dispersibility and gene delivery, iron oxide magnetic nanoparticles were prepared for delivery of miRNA34a. The iron oxide magnetic nanoparticles were delivered to TNBC cells, and their efficacy was evaluated in vitro and in vivo. Delivery of miRNA34a reduced TNBC cell migration and decreased the expression of PD-L1 at the mRNA and protein levels. In animal experiments, delivery of miRNA34a reduced tumor growth, and immunostaining and algorithmic analysis confirmed the decrease in PD-L1 expression.

Conclusion: This study is the first to modulate PD-L1 by delivering miRNA34a with magnetic nanoparticles, and the results suggest that miRNA34a can be delivered effectively using magnetic nanoparticles and has potential as a molecular imaging contrast agent.

Keywords: miRNA34a, PD-L1, Immune checkpoint protein, MRI, Theranostics, Magnetic nanoparticles, Triple-negative breast cancer

Introduction

Programmed death-ligand 1 (PD-L1) is a 40-kDa type 1 transmembrane protein that plays a major role in suppressing the immune system during events such as pregnancy, tissue allografts, autoimmune disease, and other disease states such as hepatitis. In addition, it is known that tumors use the PD-L1 pathway to suppress the antitumor immune response, and PD-L1 expression is directly linked to the survival of cancer patients (Kataoka et al. 2016; Romero 2017). For example, an analysis of 196 tumor specimens from patients with renal cell carcinoma found that high tumor expression of PD-L1 was associated with increased tumor aggressiveness and a 4.5-fold increased risk of death

(Thompson et al. 2004). Therefore, studies to regulate the expression of PD-L1, alone or in combination with conventional anticancer therapies, are receiving a lot of attention, and regulation of microRNA (miRNA)-mediated expression of PD-L1 has progressed in recent years (Thompson et al. 2004; He et al. 2015). miRNAs are small (20–22 nucleotides), endogenous, non-coding RNA molecules that act as regulators of gene expression at the post-transcriptional level through RNA interference. Mature miRNAs, which can regulate multiple target genes, associate with the 3'-untranslated regions (3'-UTRs) of specific target mRNAs to suppress translation and occasionally initiate degradation (Ha and Kim 2014; He and Hannon 2004). Also, miRNAs are actively involved in a variety of cellular processes, including differentiation, proliferation, and apoptosis. Aberrant miRNA levels affect many diseases, and in cancer, miRNAs serve as both tumor suppressors and oncogenes (Calin and Croce 2006). In 2014, it was demonstrated that miR-200 inhibited PD-L1, which prevented the epithelial-to-mesenchymal transition and metastasis in lung cancer (Chen et al. 2014). Cortez et al. investigated the role of miRNA34a in the regulation of PD-L1 activity using miRNA34a-loaded liposomes and identified a novel mechanism by which tumor immune evasion is regulated by the p53/miRNA34a/PD-L1 axis (Cortez et al. 2015). However, it is a challenge to deliver miRNA safely and efficiently deliver in vivo, and appropriate delivery systems are lacking. In recent studies, various nonviral vectors (e.g., magnetic nanoparticles, gold nanoparticles, and fluorescence molecules) have been investigated as promising carriers for simultaneous molecular imaging and gene delivery (Lee et al. 2009; Meng et al. 2010; Qian et al. 2020). The real-time monitoring of the miRNA delivery process as part of that research showed that those vectors can improve therapeutic efficacy and tumor accumulation. Before miRNA-mediated therapy can be used clinically, real-time imaging of gene delivery is needed. The visualization of the miRNA delivery process will enable clinicians to verify the therapeutic efficacy, biodistribution, and tumor accumulation of miRNA-mediated therapy. Triple-negative breast cancer (TNBC) lacks an estrogen receptor, a progesterone receptor, and a HER2/neu receptor and accounts for 10–20% of all breast tumors (Bauer et al. 2007; Brenton et al. 2005). TNBC is highly heterogeneous, is known to have multiple molecular subtypes, tends to grow aggressively, has a high probability of metastasis, and does not respond to hormone or targeted therapy such as Herceptin (Carey et al. 2007; Dent et al. 2007; Harris et al. 2006). About 20% of TNBC expresses PD-L1 and requires a new treatment strategy to regulate PD-L1 expression (Mittendorf et al. 2014). For this purpose, several inorganic formulations (e.g., magnetic nanoparticles, gold nanoparticles, and quantum dots) are being evaluated as attractive materials for miRNA delivery and imaging due to their facile surface modification, size control, and imaging modalities. Among them, magnetic nanovectors (MNVs) enable the monitoring of miRNA delivery by non-invasive and real-time magnetic resonance imaging (MRI), which can rapidly produce multi-informational high-resolution images. For such a system, miRNAs need to be reversibly packed into MNVs for transport into the cytoplasm, where they can effectively fulfill their RNAi function. Several techniques can be used to load miRNAs into MNVs, including cleavable linkers, electrostatic interactions, or incorporation into polymeric matrix composites. In this study, simple MNVs were constructed with cationic polymers for safe and effective delivery of miRNAs into iron oxide nanoparticles, a T_2 MR contrast agent. The amphiphilic polymer made the

nanoparticles water-soluble, and the cationic homopolymer poly-L-lysine (PLL) was used to load the miRNA in the outer layer of the MNVs, producing water-dispersible, magnetic, polycation, core–shell nanostructures. Delivery of miRNA34 using the MNVs inhibited TNBC cell migration and PD-L1 expression in vitro. In addition, tumor growth and PD-L1 expression were inhibited in vivo. These results demonstrate that MNVs with miRNA34a have potential as an effective theranostic system that uses PD-L1 to regulate tumor growth in cancer therapy.

Materials and methods

Materials

Polysorbate 80, 10-nm iron oxide nanoparticles, and PLL were purchased from Sigma-Aldrich (MO, USA). Phosphate-buffered saline (PBS; 10 mM, pH 7.4), Dulbecco's modified Eagle's medium, fetal bovine serum, and antibiotic–antimycotic solution were purchased from Gibco (MA, USA). MDA-MB-231 cells were purchased from the American Type Culture Collection (VA, USA). The CCK-8 assay kit was purchased from Dojindo Laboratories (MD, USA). The miRNA34a and scrambled miRNAs were purchased from Integrated DNA Technologies (IA, USA). All miRNAs were double stranded. The miRNA34a sequences were sense: 5'-UGGCAGUGUCUUAGCUGG UUGU-3' and antisense: 3'-ACCGUCACAGAAUCGACCAACA-5'. The scrambled miRNA sequences were sense: 5'-ACCAUAUUGCGCGUAUAGUCGC-3' and antisense: 3'-UGGUAUAACGCGCAUAUCAGCG-5'. Ultrapure deionized water was used for all syntheses. All other chemicals and reagents were analytical grade.

Preparation of MNVs

The MNVs were prepared from an amphiphilic polymer and cationic polymer-mediated nanoemulsion using a previously published protocol with some modifications (Yang et al. 2021). For this, 10 mg of iron oxide nanoparticles were dissolved in 2 mL of hexane, and mixed with 40 ml of deionized water containing 200 mg of polysorbate 80. The mixed solution was ultrasonicated for 15 min at 190 W in an ice-cooled bath. The organic solvent was evaporated overnight at room temperature, and the products were purified by centrifugal filtration (Centriprep YM-3, 3000 Da, Merck, MA, USA) with three cycles at 3000 rpm for 1 h. After purification, 3 mg of PLL was added and incubated for 15 min at room temperature, and various miRNAs were added. The surface charge of the MNVs with PLL and miRNA34 and the hydrodynamic size of the MNVs were analyzed by dynamic laser scattering (ELS-Z; Otsuka Electronics, OKASA, Japan). T_2 MR images and relaxivity coefficients were collected with a 9.4 T Bruker animal MRI system (Biospec 94/20 USR; Bruker Medical Systems, Karlsruhe, Germany) equipped with a 40-mm inner-diameter quadrature RF coil (RF SUC 400 1H M-BR-LIN Road; Bruker Medical Systems, Karlsruhe, Germany). The Fe ion concentration from the nanoparticles was calculated using an inductively coupled plasma-optical emission spectrometer. The MR images were coronal T_2-weighted rapid acquisitions with relaxation enhancement (repetition time = 2000 ms, echo time = 22.2 ms, slice thickness = 1.00 mm, field of view = 5.00 × 3.00 cm, flip angle = 180.0°). The T_2 value was acquired with the following sequence: coronal T_2-weighted multi-slice-multi-echo (repetition time = 2000 ms, echo time = 99 ms, slice thickness = 1.00 mm, field of view = 5.00 × 3.00 cm, flip

angle = 180.0°). The relaxivity values of R_2 were calculated using a series of T_2 values plotted as $1/T_2$ versus [Fe]. The relaxivity coefficient ($mM^{-1}\ s^{-1}$) was equal to the ratio of R_2 ($1/T_2$; s^{-1}) to MNV concentration.

Cytotoxicity

The cytotoxicity of the MNVs to MDA-MB-231 cells was evaluated using a CCK-8 cell proliferation assay kit (Dojindo Molecular Technologies, MD, USA). MDA-MB-231 cells were seeded into a 96-well plate at a density of 2×10^4 cells/well and cultured at 37 °C in a humidified atmosphere with 5% CO_2. After 24 h of incubation, the cells were treated with MNVs at various concentrations for 24 h. To test MNVs with PLL, 50 μg/mL MNVs were incubated with PLL (1.5 μg/mL) for 5 min and serially diluted twofold into nine aliquots that were administered to the MDA-MB-231 cells for 24 h. Next, the cells were treated with CCK-8 solution according to the manufacturer's instructions. Cell viability was evaluated spectrophotometrically at 450 nm using a microplate reader (SYNERGY H1 microplate reader, BioTek Instruments, VT, USA). All experiments were performed in triplicate. The concentration of PLL was determined by referring to the literature (Yun et al. 2018).

Quantitative real-time reverse transcription PCR (qRT-PCR)

The MDA-MB-231 cells were seeded in six-well plates (2.5×10^5 cells/well) and cultured at 37 °C in a humidified atmosphere with 5% CO_2. After 1 day, 3 μg/mL MNVs with 12.5, 25, or 50 pmol of miRNA34a or scrambled miRNAs were added for 24 h. The whole cells were rinsed with warm PBS twice and then detached using a cell scraper. The whole RNA was purified using a MasterPure™ RNA purification kit (Epicentre Biotechnologies, USA) according to the manufacturer's protocol. The RNA concentration was determined using a Nanodrop 2000 spectrophotometer (Thermo Fisher Scientific, MA, USA). cDNA was synthesized from 1000 ng of total RNA using a High-Capacity RNA-to-cDNA kit (Applied Biosystems, Foster City, CA, USA). qRT-PCR was performed using a SensiFAST™ SYBR® Lo-ROX kit (Bioline, Luckenwalde, Germany), and PCR was executed using a ViiA 7 Real-time PCR system (Thermo Fisher Scientific, MA, USA). PCR was performed in triplicate, and samples were normalized to glyceraldehyde 3-phosphate dehydrogenase (GAPDH) and β-actin expression levels. PCR was performed for 40 cycles as follows: 3 min initial denaturation at 95 °C, denaturation at 95 °C for 10 s each, annealing at 60 °C for 30 s each, and extension at 72 °C for 30 s, followed by 72 °C for 5 min for a final extension. The primer sequences of RT-qPCR assay were below: forward sequence: ACGCATTTACTGTCACGGTTC, reverse sequence: CGGGCCCTC TGTCTGTAGC.

Western blotting

The regulation of PD-L1 protein expression by miRNA34a delivery was confirmed using western blot analysis. MDA-MB-231 cells were seeded in six-well plates (2.5×10^5 cells/well) and cultured at 37 °C in a humidified atmosphere with 5% CO_2. After 1 day, 3 μg/mL MNVs with 12.5, 25, or 50 pmol of miRNA34a or scrambled miRNAs were administered for 24 h. The whole cells were rinsed twice with PBS and then detached using a cell scraper and lysed in RIPA buffer (Thermo Fisher Scientific, MA, USA). The protein

concentration was measured using a BCA protein assay kit (Thermo Fisher Scientific, MA, USA). Lysates were subjected to 10% SDS-PAGE gel electrophoresis, and the proteins were transferred to a polyvinylidene fluoride membrane (Life Technologies, NY, USA). The membrane was blocked with 5% bovine serum albumin for 1 h at RT and then incubated overnight with 1 μg/ml anti-PD-L1 (ab269674, Abcam, CB, UK) and 0.1 μg/ml anti-GAPDH (NB300-221, Novus Biologicals, CO, USA). After 3 washes with 1 × TBST and incubation with HRP-conjugated secondary antibodies for 2 h at RT, the reaction product was revealed with an Amersham ECL western blotting system (Cytiva, MA, USA). The western blots were analyzed using Amersham ImageQuant 800 (Cytiva, MA, USA).

Cell migration in the wound healing assay

To evaluate the wound healing inhibition effects of miRNA34a, MDA-MB-231 cells were seeded in six-well plates (2.5×10^5 cells/well) and cultured at 37 °C in a humidified atmosphere with 5% CO_2. After 1 day, the cells in the center part of the plate were scraped and washed with warm PBS to remove the detached cells. Then 3 μg/mL MNVs and 12.5 pmol of miRNA34a were added. Cell migration was observed daily using an optical microscope (CKX41, Olympus, Tokyo, Japan). The wound widths ($n = 20$) were analyzed using ImageJ software (NIH, Bethesda, MD, USA). Three independent experiments were performed.

Mouse tumor modeling

Five-week-old female athymic Balb/c nude mice (Orient Bio, Seongnam, Korea) were used for tumor xenograft experiments. The mice were retained in microisolator cages under sterile conditions and observed for at least 1 week before study initiation to ensure proper health. Temperature, lighting, and humidity were controlled centrally. Before the experiments, all mice were anesthetized with 2% isoflurane. In the orthotopic xenograft mouse model, 2×10^6 MDA-MB-231 cells were implanted into the right mammalian fat pad using a 29-gauge needle. After 3 weeks, 3 μg/mL MNVs and 12.5 pmol miRNA were injected twice a week for a total of 5 injections. The tumor volume and survival times were recorded at least 3 times a week.

Animal MR imaging

T_2-weighted MRI experiments were conducted with a 9.4 T Bruker 20-cm bore animal MRI system (Biospec 94/20 USR; Bruker Medical Systems, Karlsruhe, Germany) equipped with a 40-mm inner-diameter quadrature RF coil (RF SUC 400 1H M-BR-LIN Road; Bruker Medical Systems, Karlsruhe, Germany). For animal MRI, anesthesia was induced by 3% isoflurane and maintained with 2% isoflurane in a mixture of 70% N_2O and 30% O_2. The respiration rate was monitored with a small animal respiration pad (Model 1025 Small Animal Monitoring and Gating System; SA Instruments, Inc., Stony Brook, NY, USA), and the body temperature was supported with a warm-water tube integrated into the animal bed. The MR images were coronal T_2-weighted rapid acquisitions with relaxation enhancement (repetition time = 1800 ms, echo time = 22.2 ms, slice thickness = 0.50 mm, acquisition matrix = 274 × 200, field of view = 2.50 × 1.80 cm, flip angle = 180.0°).

Immunohistochemistry and analysis for PD-L1

Formalin-fixed, paraffin-embedded blocks were sectioned at a thickness of 1 mm and then deparaffinized and rehydrated. Sections for PD-L1 were subjected to target retrieval in the pre-treatment module of PT Link (Agilent Dako, CA, USA) at 95 °C for 20 min in FLEX Target Retrieval Solution Low pH (Agilent Dako K8004, CA, USA) according to the manufacturer's instructions. All sections were pretreated for 10 min with 3% hydrogen peroxide to quench endogenous peroxidase and then washed twice with TBS. Primary antibodies directed against PD-L1 (ab213524, Abcam, CB, UK) were diluted 1:100 and incubated with the sections for 1 h at RT. All sections were rinsed in TBS (3 × 5 min) and incubated with anti-rabbit HRP-labeled secondary antibody (Agilent Dako k4003, CA, USA) against PD-L1 primary antibodies for 20 min at RT. Visualization of the bound peroxidase was achieved by reaction for 5 min in Liquid DAB + Substrate (Agilent Dako, K3468, CA, USA). Counterstaining was achieved by reaction for 10 min in hematoxylin. The sections were dehydrated in graded ethanol, defatted in xylene replacement, and covered. Digital images were acquired at 200 × magnification using an Aperio AT2 (Leica Biosystems, Wetzlar, Germany). The positive pixel count algorithm was provided by the Aperio Image Scope program (Leica Biosystems, Wetzlar, Germany). Detailed settings are as follows: compression quality, 30; classifier neighborhood, 0; color saturation threshold, 0.04; intensity threshold (upper limit) of weak positive pixels, 220; intensity threshold (lower limit) of weak positive pixels, 175; intensity threshold (lower limit) of medium positive pixels, 100; intensity threshold (lower limit) of strong positive pixels, 0; intensity threshold of negative pixels, -1. The positivity value of PD-L1 was evaluated as follows: positivity = number of positive (no. of weak positive + no. of positive + no. of strong positive)/total number (no. of positive + no. of negative).

Statistical analysis

Data were analyzed using GraphPad Prism software (Version 5.0, GraphPad Software, Inc.). Differences between two groups were analyzed by Student's t-test. The significance of statistical results was noted by $^{*}P < 0.05$, $^{**}P < 0.01$.

Results

Characterization of MNVs

The hydrodynamic size of the MNVs was determined by dynamic light scattering to be 11.7 ± 2.3 nm (Fig. 1A). The change in surface charge of the MNVs according to the amount of cationic polymer, PLL, can be seen in Fig. 1B. The surface charge of the 3.0 μg/mL MNVs dispersed in the aqueous phase by polysorbate 80 was -13.96 ± 0.64, and as the amount of added PLL increased to 1.5, 3, 6, 9, and 12 mg, the surface charges of the particles increased to 9.06 ± 0.38, 19.86 ± 0.35, 20.99 ± 0.35, 24.80 ± 1.80, and 23.73 ± 0.99 mV, respectively. Although the amount of PLL was doubled, the increase in surface charge after 3 mg of PLL was small, indicating that the particle surface could be sufficiently coated with 3 mg of PLL. Figure 1C shows the surface charge change on the MNVs according to the use of miRNA34a. The amount of miRNA34a used was based on the Lipofectamine RNAiMAX protocol (Thermo Fisher Scientific, MA, USA). The recommended amount of RNAiMAX for a 6-well plate was 25 pmol, and miRNA34a was

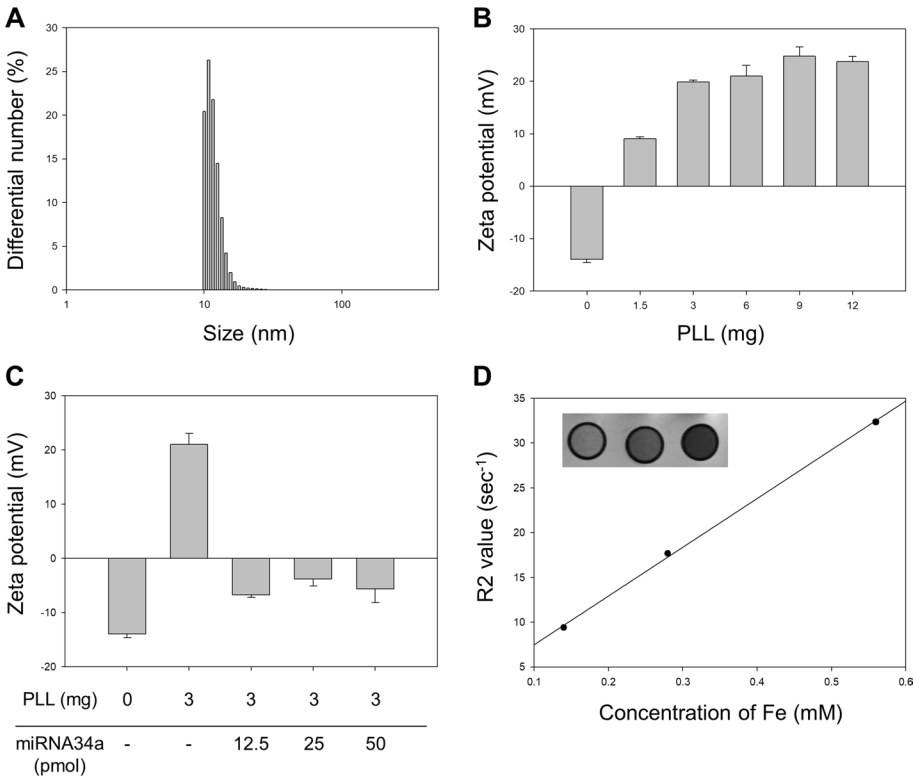

Fig. 1 Characterization of MNVs. **A** Hydrodynamic size of water-soluble MNVs. **B** Zeta potential graph of MNVs with various amounts of PLL. **C** Zeta potential graph of MNVs with various amounts of miRNA34a. **D** T2 MR image and graph showing the relaxivity coefficients around the MNVs

added to the MNVs at half or double the recommended amount of RNAiMAX. The difference in surface charge between MNVs with 12.5 and 50 pmol of miRNA34a was not large, indicating that miRNA34a was sufficiently attached to the particle surface even when only 12.5 pmol was used. To confirm the potential magnetism of the MNVs and evaluate their potential as an MR imaging contrast agent, their magnetic sensitivity was evaluated using a 9.4-T animal MRI system. As the concentration of MNVs increased, the T_2 relaxivity (R_2) of the MNVs increased linearly, with T_2 relaxivity coefficients of 11.475 mM^{-1} s^{-1} (Fig. 1D). R_2 is defined as the ratio of Fe concentration to the inverse of the T_2 relaxation time and is measured using the MR signal intensity from different T_2 relaxation times. These results indicate that MNVs were stably suspended in the aqueous phase, the PLL and miRNA34a were efficiently bound to the MNVs, and the MNVs had sufficient potential as an MRI contrast agent.

Cytotoxicity of MNVs

PLL is a representative cationic polymer and transfection agent used to deliver genes and magnetic nanoparticles to cells (Yang et al. 2021; Biray Avcı et al. 2013). In miRNA delivery, positively charged amine groups of PLL form a complex with anionic miRNA to protect the miRNA from degradation and enable cellular uptake (Höbel and Aigner 2013). To determine the cytotoxicity, MDA-MB-231 cells were exposed to various concentrations of MNVs with PLL (Fig. 2). Cytotoxicity was assessed using the CCK-8 assay

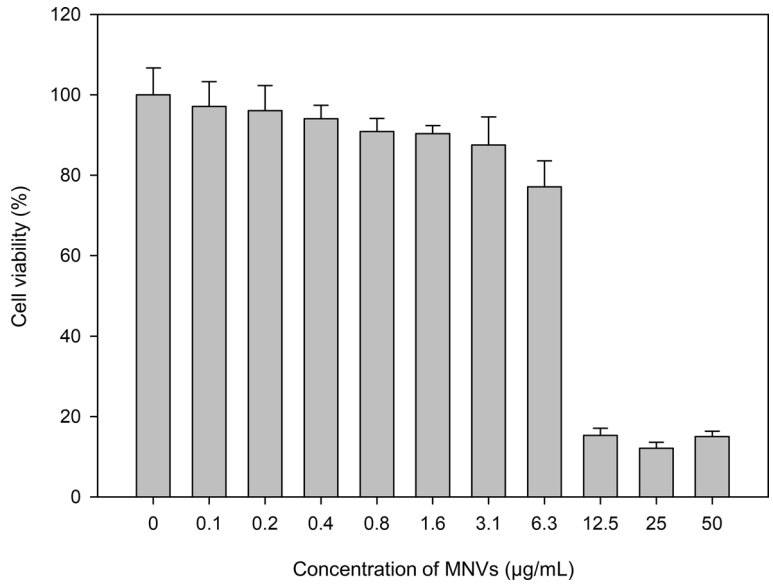

Fig. 2 Cell viability graph of MNVs with PLL

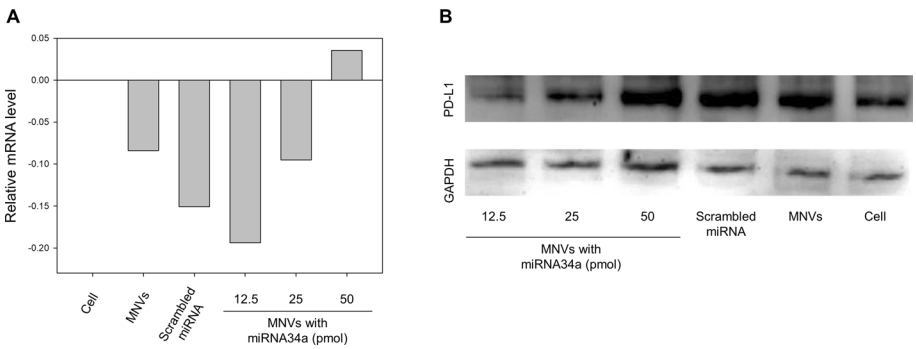

Fig. 3 qRT-PCR graph and western blot analysis. **A** qRT-PCR graph of PD-L1 mRNA under various conditions. MDA-MB-231 cells were treated with MNVs containing miRNA34a for 24 h. **B** Western blot of PD-L1 proteins under various conditions. MDA-MB-231 cells were treated with MNVs containing miRNA34a for 24 h

and 10 concentrations. The highest concentration was 50 μg/mL MNVs and 1.5 μg/ml PLL. Those concentrations were diluted twofold to make nine aliquots. Up to a concentration of 3.1 μg/mL, greater than 80% cell viability was confirmed.

Confirmation of PD-L1 suppression by miRNA34a delivery

The miRNA34a delivery by MNVs was confirmed by examining the mRNA and protein expression of PD-L1 in MDA-MB-231 cells. Three concentrations of miRNA34a were prepared for use with the same MNV concentration. Interestingly, as the amount of miRNA34a increased, the inhibitory effect on PD-L1 decreased, as shown in Fig. 3A. The most effective miRNA34a delivery did not necessarily deliver a large amount; 12.5 pmol of miRNA34a was the most effective dose for PD-L1 inhibition. Delivery of 12.5 and 25 pmoL of miRNA34a using MNVs caused approximately 19% and 9.5% reductions in PD-L1 mRNA expression, respectively. Delivery of 50 pmoL of miRNA34a using MNVs

resulted in an increase in expression of approximately 3.5%. Western blotting also confirmed that delivery of 12.5 pmol of miRNA34a using MNVs best suppressed PD-L1 protein expression (Fig. 3B). Based on the qRT-PCR and western blotting results, 12.5 pmol of miRNA34a on MNVs was considered to be the most effective dose, and subsequent experiments used those conditions.

Inhibition of tumor cell migration by miRNA34a delivery

One well-known mechanism of PD-L1 is its ability to control the invasion and migration of tumor cells. PD-L1 promotes the migration and stem cell status of renal cell carcinoma by regulating the expression of SREBP-1c, a transcription factor that increases cancer cell migration (Wang et al. 2015). PD-L1 also promotes lung cancer cells growth, migration, and invasion by targeting WIP and beta-catenin signaling (Yu et al. 2020). In nasopharyngeal cell carcinoma, overexpressed PD-L1 activates the PI3K/AKT signaling pathway to increase cancer cell migration and invasion (Fei et al. 2019). In addition, PD-L1 was reported to promote migration and invasion by upregulating Smad3 phosphorylation, which leads to activation of the TGF-β/Smad pathway and resistance to the EGFR tyrosine kinase inhibitor gefitinib in EGFR-mutant non-small cell lung cancer (Zhang et al. 2019). Therefore, measuring migration changes in tumor cells is a good way to test the effectiveness of miRNA34a delivery by MNVs. As shown in Fig. 4A, cell migration was confirmed using the wound healing assay. When miRNA34a and scrambled miRNA were delivered using MNVs, no significant change was observed in either condition after 1 day. After 2 days, all the scraped areas of cells that received MNVs with scrambled miRNA were filled with MDA-MB-231 cells. However, migration of MDA-MB-231 cells that received MNVs with miRNA34a was inhibited. In Fig. 4B, an image analysis of the inhibition of cell migration by miRNA34a delivery shows that about 34% of the wound width remained. These results indicate not only that miRNA34a was well delivered to TNBC cells using MNVs, but also that it worked well enough to affect cell migration.

Growth inhibition of an orthotopic TNBC mouse model by miRNA34a delivery

Based on the PD-L1 inhibitory effects of miRNA34a in vitro and the high correlation between PD-L1 and tumor growth, in vivo delivery of miRNA34a was expected to decrease tumor growth. Figure 5A shows how well the delivery of miRNA34a using

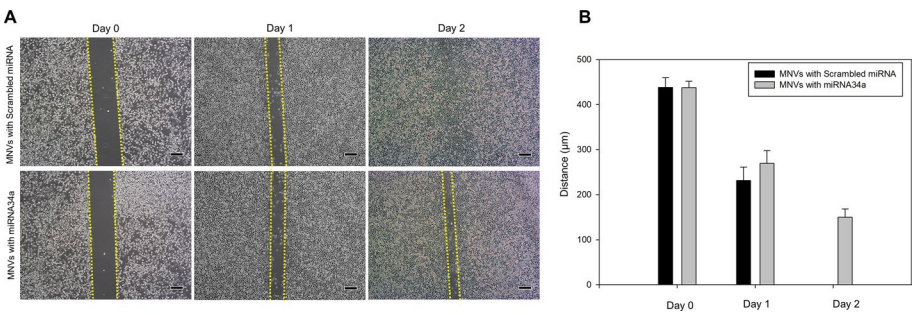

Fig. 4 Analysis of MDA-MB-231 TNBC cell migration in an in vitro wound healing assay. **A** Photos of MDA-MB-231 cells after MNV treatment (scale bar is 200 μm). **B** Graph of cell distance for each condition ($n = 20$)

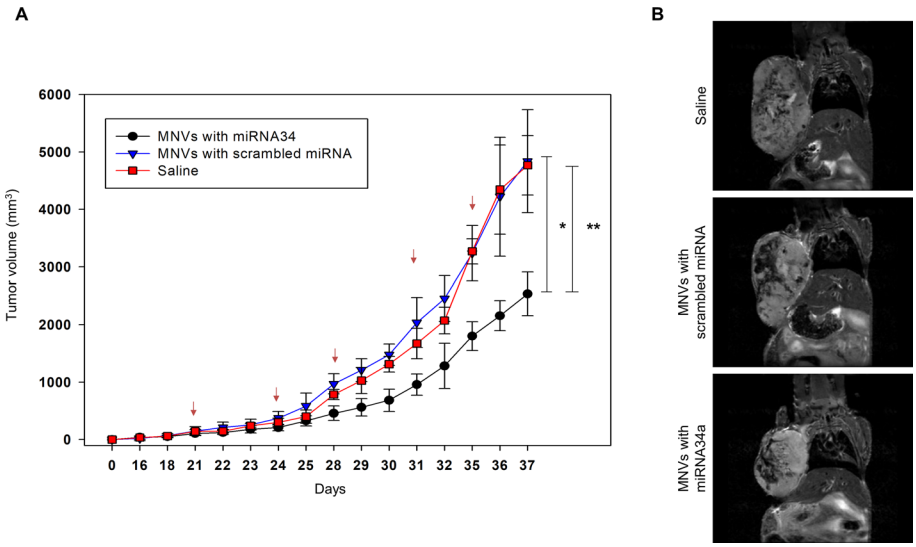

Fig. 5 Tumor growth inhibition effect of miRNA34a delivery. **A** Tumor volume graph of Balb/c nude mice (mean ± SD, n = 3). Injections were given twice a week for a total of 5 times (red arrows: days of injection). **B** MR images 37 days after tumor modeling. *P < 0.05 (vs saline), **P < 0.01 (vs MNVs with scrambled miRNA)

MNVs inhibited the growth of TNBC tumors. Tumors delivered with saline and scrambled miRNA grew to very similar sizes and reached a size requiring humane euthanasia on day 37. The average tumor volumes of groups that received TNBC cells with saline and scrambled miRNAs were 4838.6 ± 895 mm^3 and 4768.8 ± 517 mm^3, respectively. However, the average tumor volume in the groups that received miRNA34a was 2534.2 ± 378 mm^3, about 47.6% smaller than the saline group and 46.9% smaller than the scrambled miRNA group. The tumor size on day 37 is confirmed by the T_2 MR image in Fig. 5B. In addition, the contrast provided by the iron oxide nanoparticles was confirmed in all the mice injected with MNVs. These results suggest that delivering miRNA34a using MNVs effectively inhibited tumor growth and has potential as an MRI contrast agent in vivo.

Decrease in PD-L1 expression in tumor tissue via miRNA34a delivery

In an in vivo experiment, immunohistochemistry was performed on tumor tissues to confirm that delivery of miRNA34a by MNVs was effective in reducing the expression of PD-L1. As shown in Fig. 6A, the expression of PD-L1 proteins (brown dots) was confirmed over a wide range of tumor tissue treated with saline and scrambled miRNA, whereas it was significantly reduced in tumor tissue treated with miRNA34a. The positive pixel count algorithm analysis provided by the Aperio Image Scope program improves the visibility of a specific protein stain present in the immunohistochemistry images. In the image created by the positive pixel count algorithm, PD-L1 proteins are indicated by orange dots, and the expression was significantly reduced by delivery of miRNA34a. After running the positive pixel count algorithm on all mouse tumor tissues from the in vivo experiment, positivity was measured. As shown in Fig. 6B, the positivity for PD-L1 in the mouse group that received miRNA34a was lower than that in the groups treated with saline or scrambled miRNA. The PD-L1 positivity in the saline,

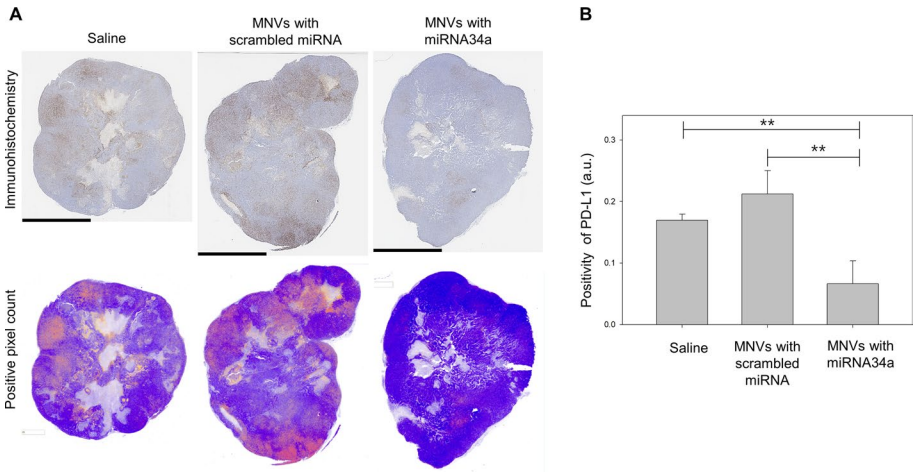

Fig. 6 Immunohistochemistry and analysis after miRNA34a delivery. **A** Immunohistochemistry and positive pixel count algorithm images for PD-L1 in each tumor. The scale bar is 4 mm. **B** The positivity graph of each tumor after processing by the positive pixel count algorithm (mean ± SD, n = 3, **P < 0.01 vs MNVs with scrambled miRNA, vs MNVs with miRNa34a)

scrambled miRNA, and miRNA34a groups was 0.17 ± 0.01, 0.21 ± 0.04, and 0.07 ± 0.04, respectively. These results indicate that miRNA34a delivery with MNVs effectively suppressed PD-L1 expression in vivo and reduced tumor growth.

Discussion

PD-L1 expression in cancerous conditions depends on the type of tumor and is intricately regulated at both the transcriptional and post-transcriptional levels. At the transcriptional level, transcription factors such as HIF-1, STAT3, NF-κB, and AP-1 regulate expression (Noman et al. 2014). In addition, PD-L1 is closely related to p53, a tumor suppressor gene. In NSCLC with a p53 mutation, a study showed that decreased miRNA34a expression increases PD-L1 expression. Most of the regulation of PD-L1 by miRNA34a targets the 3' UTR of the CD274 gene encoding PD-L1. Therefore, when miRNA34a expression is restored by delivering miRNA34a, the efficacy of radiation therapy and T-cell immunity in the tumor microenvironment are improved (Fei et al. 2019). Based on the results of several studies that showed miRNA34a to be involved in PD-L1 expression, this study created MNVs using magnetic nanoparticles and a cationic polymer, PLL, to deliver miRNA34a to TNBC cells. For decades, magnetic nanoparticles have been used as MRI contrast agents, drug carriers, and gene carriers. Because magnetic nanoparticles are generally solid, the material to be delivered is often attached to the outside of the particle. The MNVs in this study were treated with a classical and convenient method using cationic polymers to allow them to electrically carry miRNA34a. In an in vitro experiment, MNVs with miRNA34a reduced TNBC mobility and decreased PD-L1 expression at the mRNA and protein levels. At the beginning of the experiment, it was expected that as much miRNA34a as possible should be delivered to maximize the reduction in PD-L1 expression. However, delivery of too much miRNA34a was not effective in reducing PD-L1 expression. The exact mechanism for this finding is not understood. Perhaps excessive delivery of miRNA34a stimulated another signaling mechanism to maintain

PD-L1 expression in the cell. In the in vivo experiment, 5 intratumoral doses of MNVs with miRNA34a reduced tumor growth by about 47% and decreased the expression of PD-L1 protein in the tumor. It is expected that a more effective antitumor effect could be obtained by increasing the number of MNVs delivered. MNV delivery was limited to intratumoral injections, and that method needs improvement. Although it was confirmed that MNVs could regulate the expression of PD-L1 at the cellular level, it was difficult to estimate how many MNVs would accumulate in the tumor if the particles were delivered into a blood vessel. In this study, intratumoral delivery was used to confirm the concept of MNVs. Further studies on intravenous delivery of MNVs will be needed to advance and diversify therapeutic and application studies.

Conclusion

Since the discovery of PD-L1, an immune checkpoint protein, research to control its expression, alone or in combination with known treatments, has been conducted in many fields. miRNA34a, which was a potential tumor suppressor, is now considered a very good candidate for genetically modulating PD-L1. To deliver miRNA34a simply and efficiently, 10-nm iron oxide nanoparticles were selected. An amphiphilic polymer was used to improve the aqueous phase dispersibility of the nanoparticles, and a cationic polymer (PLL) was used together to make a magnetic nanovector for miRNA34a delivery. The most efficient amount of miRNA34a was verified through cell experiments. The delivery of an appropriate amount of miRNA34a suppressed the expression of PD-L1 mRNA and protein and the migration of MDA-MD-231 TNBC cells. In animal studies, delivery of miRNA34a using MNVs reduced tumor growth by approximately 47% compared with the delivery of scrambled miRNA. The immunohistochemistry results confirmed that PD-L1 expression inside the tumor was greatly reduced by miRNA34a delivery. This study showed that delivery of miRNA34a using MNVs can modulate PD-L1 expression and reduce tumor growth. Recently, many studies on PD-L1 have tested various treatment methods, such as radiation or chemotherapy, in combination with PD-L1 modulation. Using MNVs to deliver miRNA34a will have high utility value as a tool for tumor imaging and PD-L1 suppression in combination therapies.

Acknowledgements
Not applicable.

Author contributions
SHY conceived of this work, carried out experiments, and wrote the manuscript. MP technical support during all animal experiment. HYS and HWR gave technical support during western blot and qRT-PCR. HL and Y-M H supervised entire project and involved in the designing of all experiments and revised the manuscript. All authors read and approved the final manuscript.

Funding
This research was supported by the National Research Foundation of Korea(NRF) grant funded by the Korean government (NRF-2020R1I1A1A01060851, NRF-2021R1A6A3A01086846 and NRF-2022R1A2C2007490).

Availability of data and materials
The datasets used and/or analyzed during the current study are available from the corresponding author on reasonable request.

Declarations

Ethics approval and consent to participate
All animal experimental procedures were approved by the Yonsei University College of Medicine Institutional Animal Care and Use Committee and carried out in accordance with the committee's guidelines.

Consent for publication
Not applicable.

Competing interests
The authors have no other relevant affiliations or financial involvement with any organization or entity with a financial interest in or financial conflict with the subject matter or materials discussed in the manuscript.

Received: 9 August 2022 Accepted: 21 February 2023
Published: 11 March 2023

References

Bauer KR, Brown M, Cress RD, Parise CA, Caggiano V (2007) Descriptive Analysis of estrogen receptor (Er)-negative, progesterone receptor (Pr)-negative, And Her2-negative invasive breast cancer, the so-called triple-negative phenotype: a population-based study from the California cancer registry. Cancer 109:1721–1728

Biray Avcı Ç, Özcan İ, Balcı T, Özer Ö, Gþndþz C (2013) Design of polyethylene glycol-polyethylenimine nanocomplexes as non-viral carriers: Mir-150 delivery to chronic myeloid leukemia cells. Cell Biol Int 37:1205–1214

Brenton JD, Carey LA, Ahmed AA, Caldas C (2005) Molecular classification and molecular forecasting of breast cancer: ready for clinical application? J Clin Oncol 23:7350–7360

Calin GA, Croce CM (2006) Microrna signatures in human cancers. Nat Rev Cancer 6:857–866

Carey LA, Dees EC, Sawyer L, Gatti L, Moore DT, Collichio F, Ollila DW, Sartor CI, Graham ML, Perou CM (2007) The triple negative paradox: primary tumor chemosensitivity of breast cancer subtypes. Clin Cancer Res 13:2329–2334

Chen L, Gibbons DL, Goswami S, Cortez MA, Ahn YH, Byers LA, Zhang X, Yi X, Dwyer D, Lin W, Diao L, Wang J, Roybal J, Patel M, Ungewiss C, Peng D, Antonia S, Mediavilla-Varela M, Robertson G, Suraokar M, Welsh JW, Erez B, Wistuba Ii, Chen L, Peng D, Wang S, Ullrich SE, Heymach JV, Kurie JM, Qin FX (2014) Metastasis is regulated via microrna-200/Zeb1 axis control of tumour cell Pd-L1 expression and intratumoral immunosuppression. Nat Commun 5:5241

Cortez MA, Ivan C, Valdecanas D, Wang X, Peltier HJ, Ye Y, Araujo L, Carbone DP, Shilo K, Giri DK, Kelnar K, Martin D, Komaki R, Gomez DR, Krishnan S, Calin GA, Bader AG, Welsh JW (2015) Pdl1 regulation by P53 via Mir-34. Jnci J Natl Cancer Inst 108.

Dent R, Trudeau M, Pritchard KI, Hanna WM, Kahn HK, Sawka CA, Lickley LA, Rawlinson E, Sun P, Narod SA (2007) Triple-negative breast cancer: clinical features and patterns of recurrence. Clin Cancer Res 13:4429–4434

Fei Z, Deng Z, Zhou L, Li K, Xia X, Xie R (2019) Pd-L1 induces epithelial-mesenchymal transition in nasopharyngeal carcinoma cells through activation of the Pi3k/Akt pathway. Oncol Res 27:801–807

Ha M, Kim VN (2014) Regulation of microRNA biogenesis. Nat Rev Mol Cell Biol 15:509–524

Harris LN, Broadwater G, Lin NU, Miron A, Schnitt SJ, Cowan D, Lara J, Bleiweiss I, Berry D, Ellis M, Hayes DF, Winer EP, Dressler L (2006) Molecular subtypes of breast cancer in relation to paclitaxel response and outcomes in women with metastatic disease: results from Calgb 9342. Breast Cancer Res 8:R66

He L, Hannon GJ (2004) Micrornas: small RNAs with a big role in gene regulation. Nat Rev Genet 5:522–531

He J, Hu Y, Hu M, Li B (2015) Development Of Pd-1/Pd-L1 pathway in tumor immune microenvironment and treatment for non-small cell lung cancer. Sci Rep 5:13110

Høbel S, Aigner A (2013) Polyethylenimines for SiRNA And MiRNA delivery in vivo. Wiley Interdiscip Rev Nanomed Nanobiotechnol 5:484–501

Kataoka K, Shiraishi Y, Takeda Y, Sakata S, Matsumoto M, Nagano S, Maeda T, Nagata Y, Kitanaka A, Mizuno S, Tanaka H, Chiba K, Ito S, Watatani Y, Kakiuchi N, Suzuki H, Yoshizato T, Yoshida K, Sanada M, Itonaga H, Imaizumi Y, Totoki Y, Munakata W, Nakamura H, Hama N, Shide K, Kubuki Y, Hidaka T, Kameda T, Masuda K, Minato N, Kashiwase K, Izutsu K, Takaori-Kondo A, Miyazaki Y, Takahashi S, Shibata T, Kawamoto H, Akatsuka Y, Shimoda K, Takeuchi K, Seya T, Miyano S, Ogawa S (2016) Aberrant Pd-L1 expression through 3′-Utr disruption in multiple cancers. Nature 534:402–406

Lee JH, Lee K, Moon SH, Lee Y, Park TG, Cheon J (2009) All-in-one target-cell-specific magnetic nanoparticles for simultaneous molecular imaging and siRNA delivery. Angew Chem Int Ed Engl 48:4174–4179

Meng H, Liong M, Xia T, Li Z, Ji Z, Zink JI, Nel AE (2010) Engineered design of mesoporous silica nanoparticles to deliver doxorubicin and P-glycoprotein SiRNA to overcome drug resistance in a cancer cell line. ACS Nano 4:4539–4550

Mittendorf EA, Philips AV, Meric-Bernstam F, Qiao N, Wu Y, Harrington S, Su X, Wang Y, Gonzalez-Angulo AM, Akcakanat A, Chawla A, Curran M, Hwu P, Sharma P, Litton JK, Molldrem JJ, Alatrash G (2014) Pd-L1 expression in triple-negative breast cancer. Cancer Immunol Res 2:361–370

Noman MZ, Desantis G, Janji B, Hasmim M, Karray S, Dessen P, Bronte V, Chouaib S (2014) Pd-L1 is a novel direct target of Hif-1α, and its blockade under hypoxia enhanced Mdsc-mediated T cell activation. J Exp Med 211:781–790

Qian L, Liu F, Chu Y, Zhai Q, Wei X, Shao J, Li R, Xu Q, Yu L, Liu B, Liu Q (2020) Microrna-200c nanoparticles sensitized gastric cancer cells to radiotherapy by regulating Pd-L1 expression and Emt. Cancer Manag Res 12:12215–12223

Romero D (2017) Benefit with anti-Pd-L1. Nat Rev Clin Oncol 14:71–71

Thompson RH, Gillett MD, Cheville JC, Lohse CM, Dong H, Webster WS, Krejci KG, Lobo JR, Sengupta S, Chen L, Zincke H, Blute ML, Strome SE, Leibovich BC, Kwon ED (2004) Costimulatory B7–H1 in renal cell carcinoma patients: indicator of tumor aggressiveness and potential therapeutic target. Proc Natl Acad Sci U S A 101:17174–17179

Wang Y, Wang H, Zhao Q, Xia Y, Hu X, Guo J (2015) Pd-L1 induces epithelial-to-mesenchymal transition via activating Srebp-1c In renal cell carcinoma. Med Oncol 32:212

Yang S-H, Kang B, Choi Y, Rho HW, Son HY, Huh Y-M (2021) Genetic changes and growth promotion of glioblastoma by magnetic nanoparticles and a magnetic field. Nanomedicine 16:787–800

Yu W, Hua Y, Qiu H, Hao J, Zou K, Li Z, Hu S, Guo P, Chen M, Sui S, Xiong Y, Li F, Lu J, Guo W, Luo G, Deng W (2020) Pd-L1 promotes tumor growth and progression by activating Wip And **B**-catenin signaling pathways and predicts poor prognosis in lung cancer. Cell Death Dis 11:506

Yun S, Shin T-H, Lee J-H, Cho MH, Kim I-S, Kim J-W, Jung K, Lee I-S, Cheon J, Park KI (2018) Design of magnetically labeled cells (mag-cells) for in vivo control of stem cell migration and differentiation. Nano Lett 18:838–845

Zhang Y, Zeng Y, Liu T, Du W, Zhu J, Liu Z, Huang JA (2019) The Canonical Tgf-**B**/Smad signalling pathway is involved in Pd-L1-induced primary resistance to Egfr-Tkis in Egfr-mutant non-small-cell lung cancer. Respir Res 20:164

Publisher's Note